Point diffraction interferometer with a liquid crystal monopixel

Claudio Ramírez,[1] Eva Otón,[2] Claudio Iemmi,[3] Ignacio Moreno,[4] Noureddine Bennis,[2] José Manuel Otón,[2] and Juan Campos[1,*]

[1]*Depto. Física, Universidad Autónoma Barcelona, 08193 Bellaterra, Spain*
[2]*CEMDATIC, ETSI Telecomunicación, Universidad Politécnica de Madrid, Ciudad Universitaria, 28040 Madrid, Spain*
[3]*Departamento de Física. Universidad de Buenos Aires. Buenos Aires 1428, Argentina*
[4]*Depto. de Ciencia de Materiales, Óptica y Tecnología Electrónica, Universidad Miguel Hernández, 03202 Elche, Spain*
[*]*juan.campos@uab.es*

Abstract: In this work a novel point diffraction interferometer based on a variable liquid crystal wave plate (LCWP) has been implemented. The LCWP consists of a 3x3 cm^2 monopixel cell with parallel alignment. The monopixel cell was manufactured such that the electrode covers the entire surface except in a centered circular area of 50 μm of diameter. This circle acts as a point perturbation which diffracts the incident wave front giving rise to a spherical reference wave. By applying a voltage to the LCWP we can change the phase of the wave front that passes through the monopixel, except at the center. Phase shifting techniques are used in order to calculate the amplitude and phase distribution of the object wave front. The system allows a digital hologram to be obtained, and by using the Fresnel diffraction integral it is possible to digitally reconstruct the different planes that constitute the three dimensional object.

©2013 Optical Society of America

OCIS codes: (090.1995) Digital holography; (230.3720) Liquid-crystal devices; (120.3180) Interferometry; (120.5050) Phase measurement.

References and links

1. U. Schnars and W. Jüptner, "Direct recording of holograms by a CCD target and numerical reconstruction," Appl. Opt. **33**(2), 179–181 (1994).
2. I. Yamaguchi and T. Zhang, "Phase-shifting digital holography," Opt. Lett. **22**(16), 1268–1270 (1997).
3. V. Linnik, "Simple interferometer for the investigation of optical systems," Proc. Acad. Sci. USSR **1**, 208–210 (1933).
4. C. R. Mercer and K. Creath, "Liquid-crystal point-diffraction interferometer," Opt. Lett. **19**(12), 916–918 (1994).
5. C. Iemmi, A. Moreno, J. Nicolás, and J. Campos, "Evaluation and correction of aberrations in an optical correlator by phase-shifting interferometry," Opt. Lett. **28**(13), 1117–1119 (2003).
6. C. Iemmi, A. Moreno, and J. Campos, "Digital holography with a point diffraction interferometer," Opt. Express **13**(6), 1885–1891 (2005).
7. G. Wang, Y. Zheng, A. Sun, S. Wu, and Z. Wang, "Polarization pinhole interferometer," Opt. Lett. **16**(17), 1352–1354 (1991).
8. H. Kihm and Y. Lee, "Polarization point diffraction interferometer for fringe stabilization," Proc. SPIE **7790**, 779013 (2010).
9. R. M. Neal and J. C. Wyant, "Polarization phase-shifting point-diffraction interferometer," Appl. Opt. **45**(15), 3463–3476 (2006).
10. M. Paturzo, F. Pignatiello, S. Grilli, S. De Nicola, and P. Ferraro, "Phase-shifting point-diffraction interferometer developed by using the electro-optic effect in ferroelectric crystals," Opt. Lett. **31**(24), 3597–3599 (2006).
11. J. W. Goodman, Chapter IV "Fresnel and Fraunhofer diffraction" in *Introduction to Fourier Optics*, 3rd ed. (Roberts & Company, 2005).
12. M. K. Kim, "Principles and techniques of digital holographic microscopy," SPIE Rev. **1**(1), 018005 (2010).
13. U. Schnars and W. Jueptner, "Digital holography, numerical reconstruction" in *Digital Holography* (Springer Verlag, 2005), Chap. 3.2.

14. I. Moreno, A. Lizana, A. Márquez, C. Iemmi, E. Fernández, J. Campos, and M. J. Yzuel, "Time fluctuations of the phase modulation in a liquid crystal on silicon display: characterization and effects in diffractive optics," Opt. Express **16**(21), 16711–16722 (2008).
15. C. Ramirez, B. Karakus, A. Lizana, and J. Campos, "Polarimetric method for liquid crystal displays characterization in presence of phase fluctuations," Opt. Express (to be published).

1. Introduction

In digital holography several interference fringe patterns are recorded with a CCD from which the complex amplitude of the wave front is obtained. After that, it is possible to reconstruct different planes of the object by using the Kirchoff-Fresnel propagation equations [1]. Although the resolution of the CDDs is improving, they are still very far from the conventional holographic materials. Thus, the angle between the reference wave and the object wave must be small. In consequence, in the reconstruction step the non-diffracted order, the conjugate wave and the object wave are superimposed. Yamaguchi et al. [2] proposed the use of phase shifting interferometry to calculate the amplitude and phase distribution of the object wave front at the CCD plane. Thereby, no desired terms are avoided. In digital holography, most of the systems are based in a Mach-Zehnder interferometer, where reference and object wave fronts travel by different paths. This makes the interferometer more sensible to vibrations, air flows, etc. The Point Diffraction Interferometer (PDI) [3] is an in-line common path interferometer, thus more robust and compact, and that tolerates the use of partially coherent light. On the other hand, the introduction of liquid crystals permits the implementation of the interferometric methods by phase shifting [4]. In previous works [5, 6] we proposed a PDI that uses liquid crystal displays. In the first case [5], the PDI was used to measure in situ aberrations in an optical correlator. While in the second [6], the interferometer was used in digital holography applications. In the last case, the use of a pixelated display is not necessary because the phase was modified in only one pixel of the pixelated screen. So the use of a monopixel, as it is proposed on this paper, will have the advantage of using a simpler and chipper device without the need of a complicated electronic to control it. Moreover, the pixelated structure of the display creates different diffraction orders that reduce the overall efficiency of the interferometer because the light is distributed on the different replicas of the image, these replicas could also reduce the size of the non-overlapping image.

Several other works have made proposals of point diffraction interferometers by using polarization optics. Some of them [7] and more recently [8] use pinholes in polarizers and waveplates to allow the interferences to form. These proposals cannot perform phase shifting between the object and reference beams, making thus more difficult the fringe analysis. Neal and Wyant have proposed [9] a system able to perform the phase shifting. First a linear polarization state is generated and with an electro-optical modulator the relative phase between the s and p components can be varied. The point diffraction is edged in a half wave-plate at 45 degrees. By means of a polarizer the s and p components are projected to allow the interference to be formed. In [10] a simpler configuration is proposed by using a z-cut lithium niobate crystal. A thin aluminum layer is deposited on both sides and a pinhole is edged in one side. By applying a voltage the relative phase between the two beams can be changed. This device has the advantage that can be operated a very fast speed, and as the authors said the main drawback is the high voltage necessary to use in comparison with devices based on liquid crystals.

In this work we propose the fabrication and use of a liquid crystal monopixel cell with parallel alignment. The electrode covers the whole liquid crystal cell, except a circular area of 50 μm at center. When a voltage is applied the phase of the wave front that impinges on the liquid crystal is modified, except in this circular region. Therefore, this monopixel allows efficiently implementing a PDI of common path with capability of interferometry by phase shifting, without any additional artifact produced by the pixelated structure of a microdisplay.

In section 2 we explain the monopixel fabrication process. In section 3 we describe the proposed PDI and the method for calculating the amplitude and phase distribution of the object wave front. Finally, in section 4 we show the obtained experimental results.

2. Liquid crystal monopixel cell

The monopixel device is based on a liquid crystal cell having an active area of 3×3 cm2 approximately. The cell is a sandwich-like flat structure, formed by two ultra-flat glasses of 0.7 mm of thickness between which a thin layer of liquid crystal is trapped. All the process is performed in a clean room.
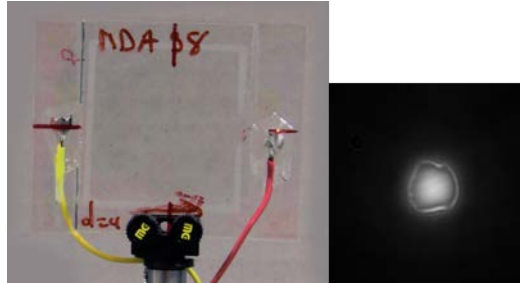

Fig. 1. Monopixel of liquid crystal wave plate (LCWP), with parallel alignment, made by Universidad Politécnica de Madrid. On the right, a magnified view of the central part to see the circular area without electrode on one of the glass plates of the monopixel.

The inner surfaces of the glasses are coated with a transparent semiconductor (Indium Tin Oxide, ITO) which acts as electrode (about 20 $\Omega/\square$). The coating on one of the glasses is left intact. In the opposite glass, a circular area of 50 μm diameter is removed by means of a photolithographic process, as is shown in Fig. 1.

Next, a polyimide layer (PIA2000, Chisso) is spin-coated onto the ITO electrode of both glasses. The polyimide (actually, the monomer) is cured in an oven to promote polymerization, and eventually is mechanically rubbed with a special lint-free cloth mounted on a cylinder onto which the glasses circulate under controlled conditions. The buffing process induces a preferential direction on the polyimide layer of the glasses, which eventually will determine the orientation of the liquid crystal layer.

Once the surface orientation is conditioned, the cell is mounted by placing the active surfaces in front to each other. Calibrated silica microspheres of 4 μm diameter are deposited on one of the surfaces, with aid of an aerograph. The microspheres act as spacers, allowing assembling the cell with a predetermined separation between the glasses. The cell edges are sealed with a serigraphed adhesive (gasket), leaving just a slit in the center of one of the edges. The glasses do not overlap fully to each other. A small lip is intentionally left on opposite sides, so that the inner surface of each glass is accessible from the outside for electrical connections.

The result of the above processes is ultimately a prismatic bottle of 3 cm × 3 cm × 4 μm. This bottle is filled, inside a vacuum chamber, with liquid crystal MDA-98 (Merck). The slit is then sealed with a photopolymerizable adhesive (NOA-65). Indium-metal contacts are soldered to the ITO electrodes of the inner surfaces, in order to apply the desired electric signals to the liquid crystal.

Surface conditioning induces the liquid crystal to orient parallel to the glass surfaces, along the predefined rubbing direction (so called homogeneous alignment). On the other hand, MDA-98 is a liquid crystal mixture having positive dielectric anisotropy (i.e., the dielectric constant along the molecular axis is higher than the dielectric constant of its perpendicular plane) and high birefringence ($\Delta n = 0.266$ @ 589 nm). The positive dielectric anisotropy will induce the liquid crystal molecules to orient their axes parallel to the electric field. The birefringence will then induce phase delays between the switched and unswitched regions of the liquid crystal cell.

Therefore, when an electric signal is applied to the electrodes, the liquid crystal molecules tend to be oriented, aligning its director axis parallel to the applied electric field (i.e., perpendicular to the glass plates). As the initial position –induced by the conditioning surface– is parallel to the glass plates, a reorientation of the liquid crystal molecules occurs,

modifying the refractive index that "sees" the light with linear polarization parallel to the orientation direction. Thus, a variable delay controlled by the external voltage is produced. The liquid crystal located inside the central circle does not switch (the electrode has been removed), so that a variable phase difference is generated between this circular area and the remaining area of the monopixel. The aspect ratio of the circle (50:4 μm diameter-thickness) is flat enough, so that the deformation effects of the electric field in the circle edges (fringing) can be considered negligible.

3. Point diffraction interferometer

The proposed PDI is based on this above described liquid crystal wave plate (LCWP). A sketch of the experimental set up is shown in Fig. 2. The laser beam is focalized in a rotating diffuser to decrease the temporal coherence. Lens L1 form the image of the point source at the plane where the LCWP is placed, just on the central spot without ITO. At this plane, the Fourier transform of the transmittance of any object placed between the lens L1 and the LCWP is formed. A circular aperture, between L1 and LCWP, is introduced to limit the beam diameter. We have introduced a variable aperture, and in the experiments that are shown the aperture was about 1 cm diameter. By means of lens L2 the image of the aperture plane is imaged onto the CCD camera. As we will see later on the mathematics we need to image some parts of the non-transmitting aperture to make an estimation of the DC term intensity. In this architecture the object wave front interferes with the wave front diffracted by the circular area in the LCWP, i.e. the light that constitutes the DC term of the Fourier transform acts as the reference beam of the interferometer. The light that impinges on the monopixel is linearly polarized by means of LP1, parallel to the director axis of the liquid crystal molecules. Quarter Wave Plate WP1 is used to change the ellipticity and orientation of the elliptically polarized light before the linear polarizer in order to control the light intensity. By rotating the WP1 the ellipticity and orientation axis of the polarized light is changed, and then the intensity of the light that passes through the polarizer LP1 also changes. This permits us to change the intensity at the CCD camera and adjust it to its dynamic range. A variable phase delay between both wave fronts can be introduced by applying the appropriate voltage on the electrodes of the LCWP. A difference with the set-up proposed by Mercer and Creat [4] is that we are using the DC term as a reference, instead of using a higher frequency component. As the DC term is rather intense in comparison with the rest of the spectrum it is not necessary to attenuate the rest of the Fourier plane, even though the area of the circular aperture is small (50 μm diameter) in comparison with the size of the spectrum (about 2 cm diameter). We obtain fringes with good contrast as can be seen below in Fig. 5.
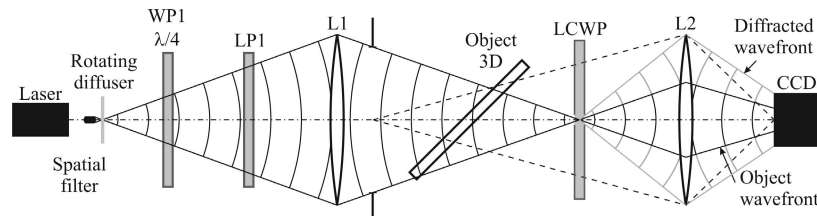

Fig. 2. Experimental setup of the Point Diffraction Interferometer. The laser beam is expanded and filtered with a spatial filter. LP1 is a linear polarizer with its transmission axis parallel to the optical axis of the LCWP. Next of the liquid crystal, a diffracted wave front is generated. Lens L2 is used to focusing one object plane (object wave) and diffracted wave (reference wave) on CCD.

The transfer function of the (LCWP) can be described as

$$H(u) = \exp\left(i\frac{2\pi n}{N}\right) + \delta(u)\left[-\exp\left(i\frac{2\pi n}{N}\right) + 1\right], \tag{1}$$

$$\delta(u) = \begin{cases} 1 & u = 0 \\ 0 & u \neq 0 \end{cases}.$$

We can rewrite Eq. (1) as

$$H(u) = \exp(i\phi_n) + \delta(u)[-\exp(i\phi_n) + 1], \tag{2}$$

where $\phi_n = \frac{2\pi n}{N}$ is the phase delay introduced at each of the N steps employed to apply the phase shifting interferometry technique.

Let us define the complex amplitude of the object wave front as

$$O(x) = o(x)\exp[i\Psi(x)]. \tag{3}$$

In this way the complex amplitude on the CCD plane can be expressed as the convolution of the object wave front with the impulse response of the (LCWP):

$$A_n(x) = O(x) * H(x). \tag{4}$$

The convolution theorem lets us rewrite Eq. (4) as

$$A_n(x) = F^{-1}\{O(u)H(u)\},$$
$$A_n(x) = F^{-1}\{O(u)[\exp(i\phi_n) + \delta(u)(-\exp(i\phi_n) + 1)]\}, \tag{5}$$
$$A_n(x) = o(x)\exp[i(\Psi(x) + \phi_n)] - [\exp(i\phi_n) - 1]F^{-1}\{O(u)\delta(u)\}.$$

If the complex constant $K = |K|\exp(i\sigma)$ is defined as the average value of O(x) then

$$A_n(x) = o(x)\exp[i(\Psi(x) + \phi_n)] - [\exp(i\phi_n) - 1]K. \tag{6}$$

Keeping in mind that the CCD detects intensity, i.e., the square modulus of the amplitude $A_n(x)$, and doing the substitution $\hat{o} = o(x)\exp[i(\Psi(x) + \phi_n)]$ yields

$$|A_n|^2 = \left|\hat{o} - [\exp(i\phi_n) - 1]K\right|^2, \tag{7a}$$

$$|A_n|^2 = |\hat{o}|^2 - \hat{o}[\exp(-i\phi_n) - 1]K^* - \hat{o}^*[\exp(i\phi_n) - 1]K + [\exp(i\phi_n) - 1][\exp(-i\phi_n) - 1]|K|^2,$$

$$|A_n|^2 = |\hat{o}|^2 \quad + 2|K|^2 + \left[-2|K|^2\cos(\phi_n) + |K|2\cos(\sigma - \Psi(x))o(x)\right]\cos(\phi_n)$$

$$- |K|2\cos[\sigma - \Psi(x)]o(x) + |K|2\sin[\sigma - \Psi(x)]\sin(\phi_n)o(x)$$

(7b)

Let us multiply the detected intensities by $\cos(\phi_n)$ and $\sin(\phi_n)$ in order to obtain the terms

$$C = \sum_{n=0}^{N-1} |A_n|^2 \cos(\phi_n)$$
$$S = \sum_{n=0}^{N-1} |A_n|^2 \sin(\phi_n). \tag{8}$$

Then, substituting Eq. (7b) into Eq. (8) and using the orthogonality properties of sinusoidal functions, the following relations can be obtained:

$$C = \frac{N}{2}\left[-2|K|^2 + |K|2\cos\left(\sigma - \Psi(x)\right)o(x)\right],$$

$$S = \frac{N}{2}\left[|K|2\sin\left(\sigma - \Psi(x)\right)o(x)\right],$$

$$C = -N|K|^2 + N|K|\cos\left[\sigma - \Psi(x)\right]o(x), \tag{9a}$$

$$S = N|K|\sin\left[\sigma - \Psi(x)\right]o(x). \tag{9b}$$

The images captured by the CCD camera contain regions that belong to the image of the aperture placed behind the lens L1. In these regions only the constant term proportional to $|K|^2$ appears, so it can be determined.

By dividing Eq. (9)a) by Eq. (9b), one obtains

$$\frac{C}{S} = \frac{-N|K|^2 + N|K|\cos\left(\sigma - \Psi(x)\right)o(x)}{N|K|\sin\left(\sigma - \Psi(x)\right)o(x)} = -\frac{|K|}{\sin\left(\sigma - \Psi(x)\right)o(x)} + \frac{\cos\left(\sigma - \Psi(x)\right)}{\sin\left(\sigma - \Psi(x)\right)},$$

$$\frac{\cos\left(\sigma - \Psi(x)\right)}{\sin\left(\sigma - \Psi(x)\right)} = \frac{C}{S} + \frac{|K|}{\sin\left(\sigma - \Psi(x)\right)o(x)} = \frac{C}{S} + \frac{N|K|^2}{S} = \frac{C + N|K|^2}{S}, \tag{10}$$

$$\tan\left(\sigma - \Psi(x)\right) = \frac{\sin\left(\sigma - \Psi(x)\right)}{\cos\left(\sigma - \Psi(x)\right)} = \frac{S}{C + N|K|^2}.$$

Finally the unknown phase of the object wave front can be recovered by solving $\Psi(x)$ from Eq. (10):

$$\Psi(x) - \sigma = -\arctan\left(\frac{S}{C + N|K|^2}\right), \tag{11}$$

where σ is a constant phase that does not affect the complex amplitude reconstruction of the object. The magnitude of the wave-front can be obtained directly from Eq. (7a) by taking the root square of the intensity registered by the CCD camera when $\phi_n = 0$, i.e. when no voltage is applied to the cell.

In the previous derivation we have assumed that the pinhole will act as delta function (see Eq. (1)), but it has a finite size. The finite size of the pinhole has several consequences, for instance: At the image plane instead to have a constant K (see Eq. (6)) we will have the Fourier Transform of the pinhole shape. The bigger the pinhole the less uniform the reference wave, and consequently the amplitude distribution estimation at the image plane will be less accurate, decreasing at the outer parts of the image. The size of the pinhole and the size of the point spread function of the lens L1 and the circular aperture should be comparable. Smaller size of the pinhole will not increase the spatial resolution and will decrease the amount of light of the reference wave, and in this case it could be necessary to decrease the amplitude transmission of the rest of the device to have good contrast on the interference fringes. A deeper study of the effect of the pinhole size is out of the scope of this paper.

4. Focusing objects placed at different planes

Once the complex amplitude is known at a given plane, it can be digitally evaluated at other parallel planes by using the Fresnel diffraction integral [11–13]:

$$O(x', y') = \frac{\exp(ikd)}{id\lambda} \iint_{\infty} \left\{ O(x, y) \exp\left[\frac{ik}{2d}\left((x'-x)^2 + (y'-y)^2\right)\right] dxdy \right\}. \quad (12)$$

Let us group terms and define h(x′, y′) as the optical transfer function at plane (x′, y′), after propagating a distance d:

$$h(x'-x, y'-y) = \frac{\exp(ikd)}{id\lambda} \exp\left[\frac{ik}{2d}\left((x'-x)^2 + (y'-y)^2\right)\right]. \quad (13)$$

The Fresnel integral (12) can be rewritten as the convolution of the complex amplitude of the object wave front O(x, y) with the optical transfer function h(x′, y′):

$$O(x', y') = \iint_{\infty} \left\{ O(x, y) h(x'-x, y'-y) dxdy \right\}. \quad (14)$$

By applying the convolution theorem in Eq. (14), one obtains

$$F\left\{O(x', y')\right\} = O\left(f_x, f_y\right) H\left(f_x, f_y\right), \quad (15)$$

where

$$O\left(f_x, f_y\right) = F\left\{O(x, y)\right\}, \quad (16)$$

$$H\left(f_x, f_y\right) = F\left\{\frac{\exp(ikd)}{id\lambda} \exp\left[\frac{ik}{2d}\left(x^2 + y^2\right)\right]\right\},$$

$$H\left(f_x, f_y\right) = \exp(ikd) \exp\left[-i\pi\lambda d\left(f_x^2 + f_y^2\right)\right]. \quad (17)$$

We use the inverse Fourier transform in order to obtain a more convenient expression to the near field propagation, due to its dependency with distance d in the phase factor. The result is

$$O(x', y') = F^{-1}\left\{O\left(f_x, f_y\right) H\left(f_x, f_y\right)\right\}, \quad (18)$$

$$O(x', y') = \exp(ikd) \cdot F^{-1}\left\{F\left[O(x, y)\right] \exp\left[-i\pi\lambda d\left(f_x^2 + f_y^2\right)\right]\right\}. \quad (19)$$

5. Experimental results

Before using the LC device in the interferometer, we have experimentally determined the axis orientation of the liquid crystal ($\alpha = 90.77°$ with respect to the laboratory vertical) and the phase delay as a function of the voltage applied between the electrodes (see Fig. 3) [14,15].

To know the voltage necessary to obtain the required phase shift, a look up table (LUT) was obtained by means of a polynomial fit of the measured phases. The electrodes of the LCWP were connected to a voltage source that applies a square bipolar signal between –V and +V at a frequency of 1 Khz. The applied voltage V can be varied by a digital to analog converter controlled by a PC.

The experimental set up is shown in Fig. 4. We used a convergent beam from a HeNe laser (λ = 632.8 nm) as light source. This beam impinges a rotating diffuser to decrease the coherence and the associated noise. A circular aperture was employed to limit the wave front extension of the laser beam. Lens L2 in Fig. 2 forms the image of this stop on the CCD camera. In this way we can calculate the constant K of Eq. (6). To test the ability of the proposed technique to focus different planes of an extended object, we placed two thin plates of glass (microscope slides denoted as Object plane 1 and 2) in separated parallel planes with
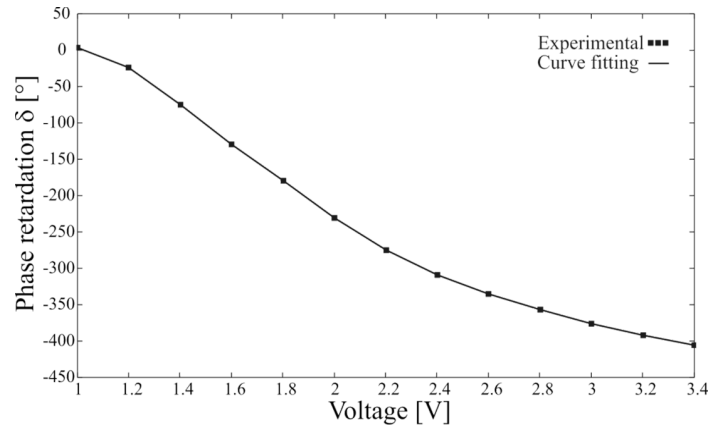
Fig. 3. LCWP phase retardation versus applied voltage. Dots indicate the experimental data, and the continuous line the corresponding polynomial fit. Negligible phase modulation is observed for values voltages below of 1 V o above of 3.4 V.
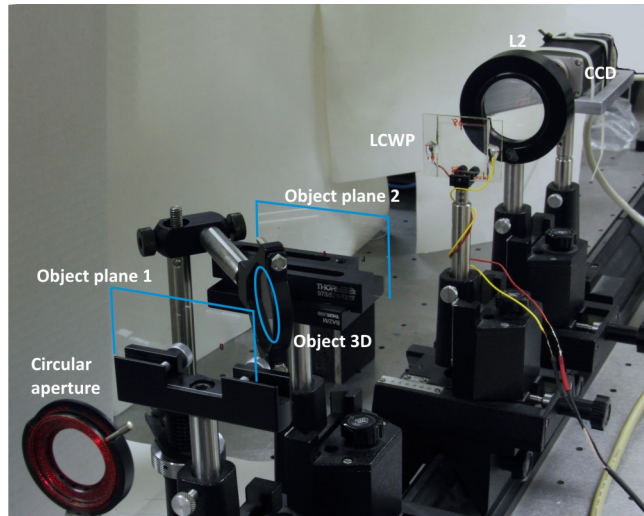

Fig. 4. Point diffraction interferometer implemented in the laboratory.

printed letters, and a reticule in diagonal (Object 3D in Fig. 4). Lenses L1 and L2 have focal length of 20 cm. Object planes 1 and 2 are separated approximately 35 cm each other. Object plane 1 is approximately 10 cm apart from Lens L1.

It should be pointed out that when there is no object in the set-up, the convergent wave front is focused on the LCWP in the circular area without electrode. In this case, the point spread function is about the same size as that of the circular area.

The four step phase shift algorithm was employed to obtain the complex distribution of the object wave front. The interferograms acquired with the CCD, for phase delays of 0, $\pi/2$, π and $3\pi/2$ between object and reference wave fronts, are shown in Fig. 5. The wrapped phase of the original wave front was evaluated by using Eqs. (8) and (11).

Figure 6 represents the magnitude and phase of the wave-front corresponding to the focused plane at the CCD camera, which coincides with the circular aperture plane of Fig. 4. One can notice (Fig. 6(a)) that the characters and the rule are defocused, while the edges of the diaphragm are on focus.
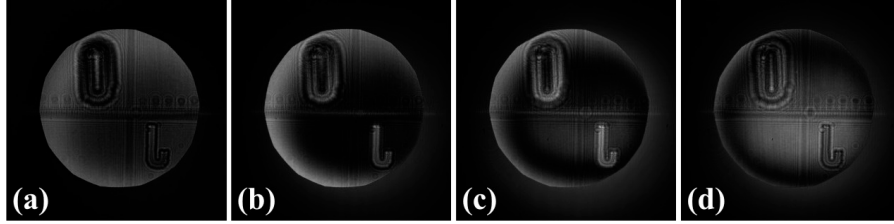
Fig. 5. Fringe patterns with phase retardance between the object and diffracted wave fronts of: (a) $\phi n = 0$, (b) $\phi n = 0.5\pi$, (c) $\phi n = \pi$ and (d) $\phi n = 1.5\pi$.
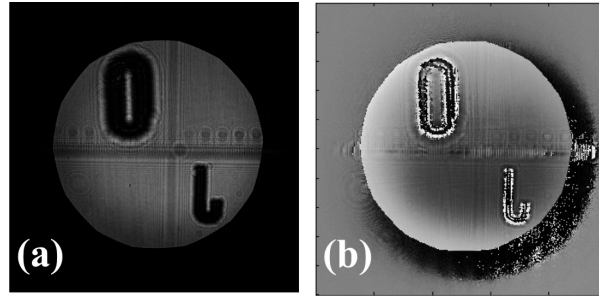

Fig. 6. (a) Magnitude of the object wave front $o(x)$, (b) calculated wrapped phase $\Psi(x)$.

By applying the Fresnel propagation Eq. (19) one can digitally focus other planes that were defocused on the original image, as is illustrated in Fig. 7. At d = 0 we obtain the result of Fig. 6(a). By selecting different planes along the z axis we can see how the successive planes are focused (first the letter J, then the reticule and the letter O). In the movie more images are taken around these planes. Therefore, these results show evidences of the proposed optical system.
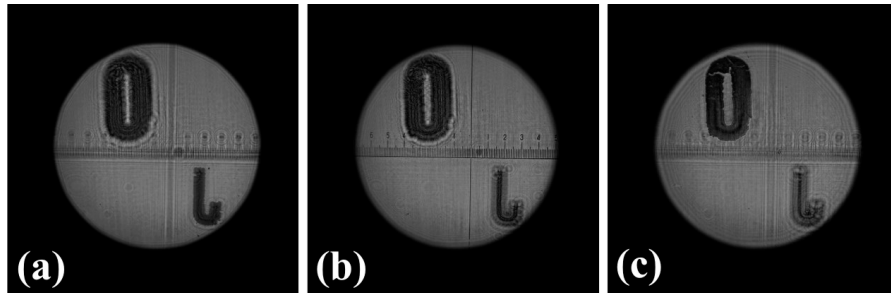

Fig. 7. Focusing different image planes using Fresnel diffraction equation: (a) d = −18.7 mm, (b) d ≈-35 mm y (c) d = −56.5 mm. (Media 1).

6. Conclusions

We have implemented a novel point diffraction interferometer (PDI) based in a liquid crystal wave plate (LCWP). In the LCWP the electrode covers whole the surface, except by a circular area of 50 μm of diameter. This area acts as a point that diffracts a wave front. The phase of the wave front that impinges on the monopixel, in contrast to the central point, is changed by applying different voltages to the LCWP. A phase shifting technique was used to obtain the amplitude and phase distribution of the object wave front. We have applied this system to obtain a digital hologram and, by digitally focusing in several planes, have used this digital hologram to reconstruct a three-dimensional object using the Fresnel diffraction integral.

Acknowledgments